Atmos. Meas. Tech. Discuss., https://doi.org/10.5194/amt-2019-132
Manuscript under review for journal Atmos. Meas. Tech.
Discussion started: 4 April 2019

Atmospheric Measurement Techniques Discussions

Aerosol measurements with shipborne sun-sky-lunar photometer and collocated multiwavelength Raman polarization lidar over the Atlantic Ocean

Zhenping Yin[1,2,3], Albert Ansmann[1], Holger Baars[1], Martin Radenz[1], Cristofer Jimenez[1], Ronny Engelmann[1], Patric Seifert[1], Alina Herzog[1], Kevin Ohneiser[1], Karsten Hanbuch[1], Luc Blarel[4], Philippe Goloub[4], Gaël Dubois[4], Stephane Victori[5], Fabrice Maupin[5]

[1]Leibniz Institute for Tropospheric Research, Permoserstraße 15, 04318 Leipzig, Germany
[2]School of Electronic Information, Wuhan University, Wuhan, China
[3]Key Laboratory of Geospace Environment and Geodesy, Ministry of Education, Wuhan, China
[4]Laboratoire d'Optique Amosphérique, Université des Sciences et Technologies de Lille, 59655 Villeneuve d'Ascq, France
[5]Cimel advanced monitoring, Paris, France

Correspondence to: Zhenping Yin (zhenping@tropos.de)

Abstract. A shipborne sun-sky-lunar photometer was tested in two trans-Atlantic cruises aboard the German research vessel *Polarstern* from 54°N to 54°S. A full diurnal cycle of mixed dust-smoke episode measured with shipborne CE318-T is presented for the first time. Latitudinal distribution of AOD from the shipborne CE318-T, Raman lidar and MICROTOPS II shows the same trend with high values at 0 ~ 20°N dust transported belt and low values at Southern Hemisphere. Coefficient of determination for the linear regression between MICROTOPS II and shipborne sun-sky-lunar photometer was 0.993 for AOD at 500 nm and 0.896 for Ångström exponent at 440-870 nm.

1 Introduction

Aerosols can influence the Earth radiation budget, e.g. by absorption and scattering of solar radiation, and modulate cloud formation and cloud microphysical properties by serving as cloud condensation nuclei (CCN) or ice nucleating particles (INP). Although great progress has been made about aerosol observations and climate modeling in recent years, the uncertainty of aerosol forcing in global climate models is still very large due to our poor understanding of aerosol global distribution and aerosol-cloud interactions (Stocker, 2014).

Most of the current aerosol observations are land-based. Although spaceborne aerosol observations are available, they cannot be used to resolve regional aerosol conditions as a function of time, e.g. to resolve the diurnal cycle of the boundary layer. Observations over the ocean is very challenging compared with land-based measurements due to the mobility of the platform and severe weather conditions. The Maritime Aerosol Network (MAN), as a component of the AErosol RObotic NETwork (AERONET), is the largest long-term aerosol observation network over the ocean (Smirnov et al., 2009). It has provided a unique dataset about aerosol optical depth (AOD) and precipitable water vapor (PWV) over the ocean even from Arctic to

Antarctica. These data is used in dust transportation research, satellite retrieval validation and atmospheric correction (Smirnov et al., 2011).

MICROTOPS II is the standard device of MAN. However, it is not dedicated for automatic maritime network observations. An operator needs to point the photometer to the Sun for a while to ensure stable measurements. Moreover, it cannot provide aerosol microphysical properties, including size distribution, scattering phase function and single scattering albedo because of missing sky radiance measurements (Smirnov et al., 2009; Smirnov et al., 2011). Therefore, a prototype of a shipborne photometer based on the most advanced sun-sky-lunar photometer technology (CE318-T), which is aimed at maritime aerosol measurement, was developed by the Laboratoire d'Optique Atmosphérique (LOA), Lille, France. This new device has all the capabilities of a land-based CE318-T (Barreto et al., 2016), like AOD measurement from 340 to 1640 nm, PWV measurement, nighttime AOD measurement and almucantar scanning measurement required for the retrieval of aerosol microphysical properties. This new instrument can also be installed on a car and conducts the measurement automatically and continuously. This prototype was tested in the framework of the OCEANET project (Macke et al., 2010) during the past two RV *Polarstern* cruises, PS113 and PS116. PS113 started at Punta Arenas, Chile on 7 May 2018 and ended at Bremerhaven, Germany on 11 June 2018. In the case of PS116, RV *Polarstern* departed from Bremerhaven on 11 November 2018 and arrived at Cape Town on 11 December 2018 (see Fig. 1 for the ship tracks). Equipped with sophisticated ground-based instruments, including a portable and automated Raman and polarization lidar system Polly^{XT} (Engelmann et al., 2016; Althausen et al., 2009), microwave radiometer, meteorological station, shadowband radiometer, full-sky imager and MICROTOPS II, it provided a unique opportunity to evaluate the capabilities of the photometer prototype and also provided useful feedback for its future developments.

This paper is organised as follows: In Sect. 2, we give a description of the shipborne CE318-T and other applied instruments and data in this paper. Then in Sect. 3.1, we present two detailed case studies to evaluate the performance of the shipborne CE318-T under pure marine conditions and lofted Saharan dust layers. Furthermore, we also present full diurnal cycle measurements to investigate the nighttime behaviour of the shipborne CE318-T by comparing the AOD values with the respective ones from Polly^{XT} observations. In Sect. 3.2, we show the comparisons between shipborne CE318-T and MICROTOPS II based on the data collected from the two RV *Polarstern* cruises. Then, we discuss the latitudinal distribution of AOD and Ångström exponent at 440-870 nm obtained during the two cruises. Finally, in Sect. 4, summarizing and concluding remarks are given.

2 Instrumentation

The instruments of the OCEANET project are scheduled for investigating aerosol cloud and radiation interactions over the remote Atlantic Ocean and contrasting northern with southern hemispheric aerosol and cloud conditions.The OCEANET project started in the fall of 2009 (Kanitz, 2012). All the instruments are mounted on the roof of the OCEANET container except the indoor Polly^{XT} lidar. The container was located on the helicopter deck, which is behind the bridge, for these two

cruises (see Fig. 2). The MICROTOPS II measurements were conducted on the bridge (see Fig. 2). It should be noted that the 'anthropogenic' smoke from the chimney could contaminate the shipborne CE318-T measurements. However, this was a compromise between avoiding strong head winds, sea spray and smoke. Nevertheless, we only found an AOD shift of 0.002 at 500 nm between shipborne CE318-T and MICROTOPS II, which shows the influence of the smoke was negligible.

2.1 Shipborne CE318-T

The prototype of the shipborne CE318-T is developed to enable AOD measurement over the mobile platform and expand the AERONET coverage to the vast ocean area (Goloub et al., 2017). In principle, the instrument is very similar to the traditional CE318-T (Barreto et al., 2016) and has nearly the same installation procedures. The apparatus consists of the optical head, rotational base, control unit, air pumping component, weather stop component, compass and GPS modules (see Fig. 3). The GPS and compass modules provide us with the coordination and orientation information, which is necessary to compensate for real-time ship movements. The air pumping module generates compressed dry-clean air to the collimator to prohibit the contamination of optical window by ambient sea spray.

The photometer arrangement is very robust and robotic to conduct 24/7 measurement without special care. The rain sensor and anemometer worked quite well as being tested under oceanic stormy and rainy weather conditions. The collected data was finally transferred to the indoor PC automatically for further analysis. This prototype has 10 channels with nominal wavelengths of 340, 380, 440, 500, 532, 670, 870, 937, 1020, 1064 nm. It can provide AOD values at nine wavelengths and PWV at both daytime and nighttime. It also has the potential of performing almucantar scanning. Further efforts and investigations would be necessary to utilise these data for aerosol microphysical research. Current data was analyzed by LOA. For the comparisons below, we take the level 1.5 products which are the currently available results from LOA.

2.2 MICROTOPS II

AOD and PWV measurements were also performed with a handheld MICROTOPS II in the framework of MAN. Spectral AODs are covered at five wavelengths (380, 440, 500, 675, 870nm). In this paper, the cloud-screened and quality assured level 2.0 data of MICROTOPS II were used for the analysis.

2.3 Polly^{XT}

The Raman polarization lidar (Polly^{XT}) was continuously operated during the entire cruise. It has 8 far-range channels with wavelengths at 355 nm (total and cross), 387 nm, 407 nm, 532 nm (total and cross), 607 nm and 1064 nm, 4 near-range channels with wavelengths at 355 nm, 387 nm, 532 nm and 607 nm (Engelmann et al., 2016). It can measure the vertical profiles of volume depolarization ratios at 355- and 532 nm, extinction coefficients at 355- and 532 nm, backscatter coefficients at 355-, 532- and 1064 nm with a 30 s and 7.5 m resolution. Hence, particle depolarization ratios at 355- and 532nm and lidar ratios at 355- and 532 nm can be retrieved (Freudenthaler et al., 2009; Baars et al., 2016). The backscatter coefficient β and extinction coefficient α are good indicators for particle concentration (Ansmann and Müller, 2005). The lidar ratio S, which is

the ratio of extinction and backscatter coefficient, describes the particle absorption ability (Müller et al., 2007; Groß et al., 2011a). Absorbing particles like soot and black-carbon-containing particles have a higher lidar ratio than non-absorbing sulfate aerosol particles. Ångström exponent Å (Angstrom, 1964) which describes the relationship between optical properties (backscatter, extinction) at two wavelengths can be used as an indicator for particle size (Baars et al., 2016; Ansmann et al., 2002). Normally, large particles like dust particles, have a small Å (< 0.5). On the contrary, small particles like biomass combustion aerosols, most continental aerosols, have a larger Å (> 1.0) (Müller et al., 2007; Baars et al., 2016; Eck et al., 1999). These intensive parameters are sensitive to particle size, shape and chemistry properties. Therefore, aerosol layers with different physical and chemical properties, like marine aerosol, dust and smoke, can be characterized based on these retrieving results.

The Polly^{XT} lidar was equipped with a near-range telescope, and the incomplete overlap zone can be suppressed to 120 m, which enabled us to capture the aerosol distribution and evolution inside the marine boundary layer (MBL) (Kanitz et al., 2013; Engelmann et al., 2016). In order to avoid the damage for the photon-counting detectors from strong solar radiation, the lidar system was turned off when the solar elevation angle exceeded 70° and the 407 nm channel was turned off routinely at daytime.

2.4 Supplementary instruments and data sources

Temperature, pressure and relative humidity (RH) profiles were obtained from radiosonde ascents. The radiosondes were launched on board the RV *Polarstern* at 11:00 UTC on each day. In order to have better temporal resolved meteorological information, Global Data Assimilation System 1° resolution (GDAS1) meteorology data (Kanamitsu, 1989) was used in the lidar data analysis. This data is calculated every three hours per day with a spatial resolution of 1° (latitude, longitude) by an atmospheric model provided by National Centers for Environmental Prediction (NCEP). In addition, the Hybrid Single-Particle Lagrangian Integrated Trajectory (HYSPLIT) model (Draxler, 2011) was used for backward trajectory analysis.

3 Results

3.1 Case studies

In order to illustrate the aerosol vertical distribution over the Atlantic Ocean and investigate the behavior of shipborne CE318-T at different aerosol conditions, we present the results from shipborne CE318-T, lidar and MICROTOPS II observations at pure marine condition and in cases with Saharan dust outbreaks. Moreover, the full diurnal cycle of AOD observations over the Atlantic Ocean can also be recorded with the shipborne photometry. Detailed analysis was applied based on the diurnal measurements from the shipborne CE318-T and Polly^{XT} lidar and daytime measurements from MICROTOPS II.

Atmos. Meas. Tech. Discuss., https://doi.org/10.5194/amt-2019-132
Manuscript under review for journal Atmos. Meas. Tech.
Discussion started: 4 April 2019

3.1.1 Marine aerosol conditions

On 23 November 2018, RV *Polarstern* was west of Western Sahara and approaching Cape Verde. Northwestern airflow and clean marine conditions prevailed. The measurements from shipborne CE318-T and lidar are shown in Fig. 4. According to the 532 nm attenuated backscatter, typical marine aerosol conditions were observed. The 532 nm volume depolarization ratio was less than 0.05 below 1.8 km, which means that the marine boundary layer was dominated by spherical sea salt particles. The backward trajectories in Fig. 5 show that the air mass was mainly carried over the ocean during the past 4 days. Furthermore, no strong aerosol layers were observed above 2 km height. The mean AOD at 532 nm from 08:30 to 11:00 UTC based on shipborne CE318-T measurements was 0.06 ± 0.01 and mean Ångström exponent at 440-870 nm was 0.26 ± 0.03, These are typical values for marine aerosols, which are dominated by coarse mode sea salt particles (Smirnov et al, 2006). The mean AOD at 532 nm and mean Ångström exponent at 440-870 nm from MICROTOPS II were 0.05 ± 0.01 and 0.20 ± 0.03, which are in good agreement with the shipborne CE318-T.

Detailed height-resolved aerosol information is displayed in Fig. 6. According to the RH profile in Fig. 6d, the marine layer reached to about 2 km height. The mean extinction coefficient was 38.5 Mm^{-1}, 27.4 Mm^{-1} and 19.2 Mm^{-1} at 355 nm, 532 nm and 1064 nm, by using Fernald method (Fernald et al., 1972) and assuming a fixed lidar ratio of 20 sr (Groß et al., 2011a; Groß, 2011). The particle depolarization ratios below 1.6 km were less than 0.02 at 355 nm and 532 nm. From 1.7 km to 2.0 km, the particle depolarization ratio increased with peak value at 355 nm (532 nm) to be 0.09 (0.08) and RH decreased to 10 % according to the GDAS1 data. These are good indicators for dried sea salt particles (Haarig et al., 2017; Bohlmann et al., 2018). When RH drops below 45 %, the spherical marine aerosol particles start to crystallize and become cubic-like in shape. These cubic dry sea salt particles will introduce a relatively strong depolarized signal and lead to the increase of particle depolarization ratio.

3.1.2 Saharan dust

When the RV *Polarstern* approached Cape Verde Islands, a dust outbreak was observed from 27 May to 31 May 2018. The whole event started with a mixture of dust and smoke above the MBL. Since 30 May 2018, the layer was lofted to 1.5 km and started to be dominated by pure Saharan dust particles.

The MICROTOPS II, shipborne CE318-T and lidar measurements from 16:00 to 17:00 UTC on 30 May 2018 are displayed in Fig. 7. According Fig. 7a, the results from the shipborne CE318-T and MICROTOPS II agreed well with mean AOD of 0.66 ± 0.03 and 0.62 ± 0.02 and mean Ångström exponent at 440-870 of 0.08 ± 0.02 and 0.07 ± 0.01. Both results indicate the presence of a large amount of large dust particles. In Fig 7c, we can see a layer, located between 0.6 km to 1 km causing slightly enhanced volume depolarization ratio and a dust layer located between 1.5 and 5 km with large volume depolarization ratio. Inside the MBL, the volume depolarization ratio was quite low which indicates that the contamination caused by dust sedimentation was small.

In Fig. 8, we present the averaged vertical profiles from lidar. The extinction coefficient was retrieved by Fernald method with assuming the lidar ratios of 60 sr (355 nm), 45 sr (532 nm) and 54 sr (1064 nm) for the dust layer and 25 sr (355, 532, 1064 nm) for the MBL. The lidar ratios at 355 and 532 nm were selected based on nighttime Raman retrieving results, and the lidar ratio at 1064 nm was from AERONET measurements (Shin et al., 2018). Meanwhile, reference values were tuned to achieve the best agreement of AOD between lidar and shipborne CE318-T. Inside the MBL, the mean extinction coefficients at 355 nm and 532 nm are 245 Mm^{-1} and 241 Mm^{-1} according to Fig. 8a, which is very large compared to pure marine conditions in Sect. 3.1.1. This might be caused by the loading and hygroscopic growth of anthropogenic aerosols. This assumption is corroborated by the backward trajectories in Fig. 9a, because a branch of the backward trajectories arriving at 500 m can be traced back to European continent. The lofted dust layer extended from 1.5 to 5 km with mean extinction coefficients at 355 nm, 532 nm and 1064 nm to be 166 Mm^{-1}, 161 Mm^{-1} and 159 Mm^{-1} and particle depolarization ratios at 355 nm and 532 nm to be 0.21 ± 0.05 and 0.31 ± 0.05, which are in good agreement with optical properties for pure Saharan dust (Groß et al., 2011a; Groß et al., 2011b; Tesche et al., 2009). The backward trajectories in Fig. 9b showed the air mass at 4 km originated from Chad, Libya and Sudan, and travelled 5 days from these regions before reaching RV *Polarstern*. A relatively clean layer can be found between the lofted dust layer and MBL with extinction coefficient and particle depolarization ratio less than 25 Mm^{-1} and 0.04, respectively. Therefore, we are convinced that the sedimentation of dust particles was negligible. Above the MBL, from 0.5 km to 1 km, there was an aerosol layer with enhanced particle depolarization ratio at 355 nm (532 nm) of 0.11 (0.15). The backward trajectories for this layer was similar with Fig. 9a. Therefore, it probably consisted of relatively dry aged anthropogenic particles or mixture of dry aged anthropogenic particles and dry sea salt particles.

3.2.3 Diurnal measurements from shipborne CE318-T and Polly^{XT}

This shipborne CE318-T has the capability to conduct nighttime measurement. This feature can help us to investigate the diurnal evolution of marine aerosols and dust layers over the ocean. However, this function is more challenging than the daytime measurement as moon tracking is much more sensitive to errors of the leveling adjustment and coordination and orientation data. Therefore, we need to further address how accurate the nighttime measurement are. In Fig. 10, we present the full diurnal measurements from the shipborne CE318-T, Polly^{XT} and MICROTOPS II at 26 November 2018. On this day, RV *Polarstern* had just passed Cape Verde and was heading towards Cape Town. A mixed layer of dust and pollution aerosol was observed over the whole day. This finding is corroborated by the 532 nm volume linear depolarization ratio plot in Fig. 10c and backward trajectories in Fig. 11. The backward trajectories shows that the air mass between 1 and 3 km on 26 November 2018 originated from the Saharan desert and were over Chad and Niger six days before crossing RV *Polarstern*. Only the trajectories for arrival height of 500 m was probably free of pollution. All the backward trajectories including the ones for 500 m and 1000 m arrival height crossed the active biomass burning regions two days before arriving RV *Polarstern*. Therefore, the advected dust layer probably took up a large amount of biomass-burning aerosols over central Africa. In order to evaluate the shipborne CE318-T AOD measurements at nighttime, AOD from Polly^{XT} was calculated based on the extinction coefficient retrieved with Raman method (Ansmann et al., 1992). Above 1.5 km, the extinction coefficient was taken from far-range

channel result and between 0.3 and 1.5 km, the near-range retrieving results was used. Below 0.3 km, the extinction coefficient was considered to be constant, as displayed in Fig. 12b. The time series of AOD can be found in Fig. 10a. The deviation between nighttime shipborne CE318-T and lidar observations was less than 0.03. Daytime measurements from the shipborne CE318-T are also in good agreement with MICROTOPS II at 11:00 UTC with a deviation of 0.01 and 0.01 for the 500 nm AOD and the Ångström exponent respectively.

The mean AOD at 532 nm is 0.42 ± 0.02 between 00:00 and 07:00 UTC. The Ångström exponent at 440-870 nm increased from 0.15 to 0.40 during this period, which indicates that the fraction of large particles decreased. A similar pattern was also found for the extinction-related Ångström exponent 355-532 nm derived from lidar data (the result is not shown here).

Further detailed vertical information can be found in Fig. 12. The top of the MBL was 350 m according to the radiosonde RH and temperature profiles in Fig. 12f. The particle depolarization ratios at 355 and 532 nm inside the MBL were 0.17 ± 0.09 and 0.12 ± 0.06 and the lidar ratios at 355 and 352 nm inside the MBL were 40.19 ± 7.03 sr and 44.76 ± 3.84 sr. These values are similar to those in the lofted mixed dust layer between 1.5 and 2.5 km and quite different from typical values for pure marine conditions in Sect 3.1.1. Therefore, we can conclude that the MBL was contaminated by the transported dust and smoke particles.

3.2 Comparisons between shipborne CE318-T, MICROTOPS II and Polly^{XT}

The AOD measurements were conducted with MICROTOPS II, Polly^{XT} and shipborne CE318-T simultaneously at daytime and with Polly^{XT} and shipborne CE318-T at nighttime. In Fig. 13, the latitudinal distribution of AOD at 500 nm (532 nm) from these three instruments is displayed for the data collected during the two RV *Polarstern* cruises, PS113 and PS116. In order to calculate the AOD with lidar measurements, Fernald method (Fernald et al., 1972) was used for retrieving the daytime results, in which lidar ratios of 20 sr (20 and 20 sr), 50 sr (50 and 50 sr) were used for marine aerosols and dust at 355 nm (532 and 1064 nm) (Groß, 2011; Groß et al., 2011a). The Raman method (Ansmann et al., 1990; Ansmann et al., 1992) was used to compare the nighttime results. For the height range with incomplete overlap, the extinction coefficient was considered to be constant. In both Fig. 13a and Fig. 13b, all measurements show the same trend with peak values between 0° and 20°N (Kanitz et al., 2013), which is the outflow region of Saharan dust and as well as large amount of biomass-burning aerosols. For PS113, this belt was mainly filled with dust particles, because the Ångström exponent at 440-870 nm was less than 0.4. However, for PS116, the air mass in this belt showed a mixture of dust and smoke because the Ångström exponent at 440-870 nm was larger than 1 (Baars et al., 2012). This finding is corroborated by the lidar measurements and backward trajectories. The southern hemisphere contains less anthropogenic aerosols and dust. Marine aerosol dominates. Nevertheless, lofted biomass burning aerosols from Brazil at 25°S during PS113 was also captured by Polly^{XT} with a layer top height of 2 km, which is not shown here.

In order to evaluate the reliability and data quality of the shipborne CE318-T, we show a correlation between MICROTOPS II AOD and shipborne CE318-T AOD in Fig. 14a. Good agreement between the shipborne CE318-T and MICROTOPS II AODs with R^2 (coefficient of determination) of 0.993 for the 500 nm AOD and of 0.896 for the Ångström exponent was found.

The deviation of AOD between those two instruments increases during severe dust outbreaks but still was below 0.03. The Ångström exponent is quite sensitive to the measurement error at clean conditions with AOD less than 0.05. Therefore the scatter in the respective correlation in Fig. 14b is acceptable.

4 Conclusions

Shipborne CE318-T measurements were conducted during two trans-Atlantic RV *Polarstern* cruises together with collocated Polly^{XT} lidar and independent MICROTOPS II. The shipborne CE318-T has a special design to avoid contamination of sea-spray and achieved the goal of automatic measurement over the ocean during the entire 4-5 weeks periods of the two cruises. Good agreement was found between the different measurements. For nighttime measurements, deviations between the 532 nm AOD observed with Polly^{XT} and the shipborne CE318-T was found to be less than 10 %. However, we found that nighttime measurements with the shipborne CE318-T are very sensitive to errors in the leveling adjustment and the compass data, Thus, great care must be taken when setting up the system. A very good compass calibration is required as well. These issues need to be tackled or mitigated in future development.

The almucantar scanning option will also be implemented in near future, which allow the retrieval of aerosol microphysical properties over the ocean. All of these features will significantly increase our potential to characterize marine aerosol distribution over the remote ocean and the impact of continental dust, smoke, and haze outbreaks on the aerosol conditions far away from the continent, as well as dust transportation and dust sedimentation over the less exploited oceans.

Data availability. Radiosonde and lidar data for the two cruises are available at the Leibniz Institute for Tropospheric Research and can be accessed upon request. MICROTOPS II data can be downloaded from the AERONET MAN database (MAN, 2019). The shipborne CE318-T data can be accessed through contact with Philippe (philippe.goloub@univ-lille.fr).

Author contributions. ZP performed the lidar data analysis and prepared the manuscript supported by AA. MR, CJ and ZP set up the instruments for PS113 and were responsible for the lidar measurements. AH, KO and KH set up the instruments during PS116 and were responsible for the lidar measurements during PS116. PG, LB, GD, SV and FM built up the prototype of the shipborne CE318-T and were responsible for the corresponding data analysis. All authors contributed to scientific discussion and in this way to the manuscript preparation.

Competing interests. The authors declare that they have no conflict of interests.

Acknowledgements. The authors acknowledge funding from ACTRIS under grant agreement no. 262254, ACTRIS-2 under grant agreement no. 654109 from the European Union's Horizon 2020 research and innovation programme, Labex CaPPA (The CaPPA project (Chemical and Physical Properties of the Atmosphere) and ESA/IDEAS program. We sincerely thank the Alfred Wegener Institute and the RV *Polarstern* crewmembers for their huge support and effort in PS113 and PS116 (acknowledgement no. AWI_PS113_00, AWI_PS116_00). We also appreciate the effort of the AERONET MAN, HYSPLIT

teams to provide the additional research data to solid the analysis in the paper. Besides, Zhenping Yin appreciates the support from the Chinese Scholarship Council (CSC) to conduct this research under the CSC no. 201706270117.

References

Althausen, D., Engelmann, R., Baars, H., Heese, B., Ansmann, A., Müller, D., and Komppula, M.: Portable Raman lidar PollyXT for automated profiling of aerosol backscatter, extinction, and depolarization, Journal of Atmospheric and Oceanic Technology, 26, 2366-2378, https://doi.org/10.1175/2009jtecha1304.1, 2009.

Angstrom, A.: The Parameters of Atmospheric Turbidity, Tellus, 16, 64-75, https://doi.org/10.1111/j.2153-3490.1964.tb00144.x, 1964.

Ansmann, A., Riebesell, M., and Weitkamp, C.: Measurement of atmospheric aerosol extinction profiles with a Raman lidar, Opt. Lett., 15, 746-748, https://doi.org/10.1364/OL.15.000746, 1990.

Ansmann, A., Riebesell, M., Wandinger, U., Weitkamp, C., Voss, E., Lahmann, W., and Michaelis, W.: Combined Raman Elastic-Backscatter Lidar for Vertical Profiling of Moisture, Aerosol Extinction, Backscatter, and Lidar Ratio, Appl Phys B-Photo, 55, 18-28, https://doi.org/10.1007/Bf00348608, 1992.

Ansmann, A., Wagner, F., Müller, D., Althausen, D., Herber, A., von Hoyningen-Huene, W., and Wandinger, U.: European pollution outbreaks during ACE 2: Optical particle properties inferred from multiwavelength lidar and star-Sun photometry, Journal of Geophysical Research: Atmospheres, 107, AAC 8-1-AAC 8-14, https://doi.org/10.1029/2001jd001109, 2002.

Ansmann, A., and Müller, D.: Lidar and atmospheric aerosol particles, in: Lidar, Springer, 105-141, 2005.

Baars, H., Ansmann, A., Althausen, D., Engelmann, R., Heese, B., Muller, D., Artaxo, P., Paixao, M., Pauliquevis, T., and Souza, R.: Aerosol profiling with lidar in the Amazon Basin during the wet and dry season, J Geophys Res-Atmos, 117, https://doi.org/10.1029/2012jd018338, 2012.

Baars, H., Kanitz, T., Engelmann, R., Althausen, D., Heese, B., Komppula, M., Preissler, J., Tesche, M., Ansmann, A., Wandinger, U., Lim, J. H., Ahn, J. Y., Stachlewska, I. S., Amiridis, V., Marinou, E., Seifert, P., Hofer, J., Skupin, A., Schneider, F., Bohlmann, S., Foth, A., Bley, S., Pfuller, A., Giannakaki, E., Lihavainen, H., Viisanen, Y., Hooda, R. K., Pereira, S. N., Bortoli, D., Wagner, F., Mattis, I., Janicka, L., Markowicz, K. M., Achtert, P., Artaxo, P., Pauliquevis, T., Souza, R. A. F., Sharma, V. P., van Zyl, P. G., Beukes, J. P., Sun, J. Y., Rohwer, E. G., Deng, R. R., Mamouri, R. E., and Zamorano, F.: An overview of the first decade of Polly(NET): an emerging network of automated Raman-polarization lidars for continuous aerosol profiling, Atmospheric Chemistry and Physics, 16, 5111-5137, https://doi.org/10.5194/acp-16-5111-2016, 2016.

Barreto, A., Cuevas, E., Granados-Munoz, M. J., Alados-Arboledas, L., Romero, P. M., Grobner, J., Kouremeti, N., Almansa, A. F., Stone, T., Toledano, C., Roman, R., Sorokin, M., Holben, B., Canini, M., and Yela, M.: The new sun-sky-lunar Cimel CE318-T multiband photometer - a comprehensive performance evaluation, Atmospheric Measurement Techniques, 9, 631-654, https://doi.org/10.5194/amt-9-631-2016, 2016.

Bohlmann, S., Baars, H., Radenz, M., Engelmann, R., and Macke, A.: Ship-borne aerosol profiling with lidar over the Atlantic Ocean: from pure marine conditions to complex dust-smoke mixtures, Atmospheric Chemistry and Physics, 18, 9661-9679, https://doi.org/10.5194/acp-18-9661-2018, 2018.

Draxler, R. R.: Hysplit (hybrid single-particle lagrangian integrated trajectory) model access via NOAA ARL ready website, https://ready.arl.noaa.gov/HYSPLIT.php, 2011.

Eck, T. F., Holben, B. N., Reid, J. S., Dubovik, O., Smirnov, A., O'Neill, N. T., Slutsker, I., and Kinne, S.: Wavelength dependence of the optical depth of biomass burning, urban, and desert dust aerosols, J Geophys Res-Atmos, 104, 31333-31349, https://doi.org/10.1029/1999jd900923, 1999.

Engelmann, R., Kanitz, T., Baars, H., Heese, B., Althausen, D., Skupin, A., Wandinger, U., Komppula, M., Stachlewska, I. S., Amiridis, V., Marinou, E., Mattis, I., Linne, H., and Ansmann, A.: The automated multiwavelength Raman polarization and water-vapor lidar Polly(XT): the neXT generation, Atmospheric Measurement Techniques, 9, 1767-1784, https://doi.org/10.5194/amt-9-1767-2016, 2016.

Fernald, F. G., Herman, B. M., and Reagan, J. A.: Determination of aerosol height distributions by lidar, Journal of Applied meteorology, 11, 482-489, https://doi.org/10.1175/1520-0450(1972)011%3C0482:doahdb%3E2.0.co;2, 1972.

Freudenthaler, V., Esselborn, M., Wiegner, M., Heese, B., Tesche, M., Ansmann, A., Muller, D., Althausen, D., Wirth, M., Fix, A., Ehret, G., Knippertz, P., Toledano, C., Gasteiger, J., Garhammer, M., and Seefeldner, M.: Depolarization ratio profiling at several wavelengths in pure Saharan dust during SAMUM 2006, Tellus Series B-Chemical and Physical Meteorology, 61, 165-179, https://doi.org/10.1111/j.1600-0889.2008.00396.x, 2009.

Goloub, P., Blarel, L., Dubios, G., Popovici, I., Podvin, T., Torres, B., Victori, S., Maupin, F., and Pikridas, M.: Current results on mobile system prototype development for Aerosol Cal/Val activities, ESA/IDEAS Project WP 3440-1/3/5, 12 Dec, 2017, 2017.

Groß, S., Tesche, M., Freudenthaler, V., Toledano, C., Wiegner, M., Ansmann, A., Althausen, D., and Seefeldner, M.: Characterization of Saharan dust, marine aerosols and mixtures of biomass-burning aerosols and dust by means of multi-wavelength depolarization and Raman lidar measurements during SAMUM 2, Tellus B: Chemical and Physical Meteorology, 63, 706-724, https://doi.org/10.3402/tellusb.v63i4.16369, 2011a.

Groß, S., Wiegner, M., Freudenthaler, V., and Toledano, C.: Lidar ratio of Saharan dust over Cape Verde Islands: Assessment and error calculation, Journal of Geophysical Research: Atmospheres, 116, https://doi.org/10.1029/2010JD015435, 2011b.

Groß, S. M.: Aerosol characterization by multi-wavelength Raman-and depolarization lidar observations, lmu, 2011.

Haarig, M., Ansmann, A., Gasteiger, J., Kandler, K., Althausen, D., Baars, H., Radenz, M., and Farrell, D. A.: Dry versus wet marine particle optical properties: RH dependence of depolarization ratio, backscatter, and extinction from multiwavelength lidar measurements during SALTRACE, Atmospheric Chemistry and Physics, 17, 14199, https://doi.org/10.5194/acp-2017-545, 2017.

Kanamitsu, M.: Description of the NMC global data assimilation and forecast system, Weather and Forecasting, 4, 335-342, https://doi.org/10.1175/1520-0434(1989)004%3C0335:dotngd%3E2.0.co;2, 1989.

Kanitz, T.: Vertical distribution of aerosols above the Atlantic Ocean, Punta Arenas (Chile), and Stellenbosch (South Africa). Characterization, solar radiative effects and ice nucleating properties, https://doi.org/10.14279/depositonce-3386, 2012.

Kanitz, T., Ansmann, A., Engelmann, R., and Althausen, D.: North-south cross sections of the vertical aerosol distribution over the Atlantic Ocean from multiwavelength Raman/polarization lidar during Polarstern cruises, J Geophys Res Atmos, 118, 2643-2655, https://doi.org/10.1002/jgrd.50273, 2013.

Macke, A., Kalisch, J., Zoll, Y., and Bumke, K.: Radiative effects of the cloudy atmosphere from ground and satellite based observations, EPJ Web of Conferences, 2010, 83-94,

MAN: AERONET Maritime Aerosol Network database, 2019.

Müller, D., Ansmann, A., Mattis, I., Tesche, M., Wandinger, U., Althausen, D., and Pisani, G.: Aerosol-type-dependent lidar ratios observed with Raman lidar, Journal of Geophysical Research: Atmospheres, 112, https://doi.org/10.1029/2006jd008292, 2007.

Shin, S. K., Tesche, M., Kim, K., Kezoudi, M., Tatarov, B., Muller, D., and Noh, Y.: On the spectral depolarisation and lidar ratio of mineral dust provided in the AERONET version 3 inversion product, Atmospheric Chemistry and Physics, 18, 12735-12746, https://doi.org/10.5194/acp-18-12735-2018, 2018.

Smirnov, A., Holben, B. N., Slutsker, I., Giles, D. M., McClain, C. R., Eck, T. F., Sakerin, S. M., Macke, A., Croot, P., Zibordi, G., Quinn, P. K., Sciare, J., Kinne, S., Harvey, M., Smyth, T. J., Piketh, S., Zielinski, T., Proshutinsky, A., Goes, J. I., Nelson, N. B., Larouche, P., Radionov, V. F., Goloub, P., Moorthy, K. K., Matarrese, R., Robertson, E. J., and Jourdin, F.: Maritime Aerosol Network as a component of Aerosol Robotic Network, J Geophys Res-Atmos, 114, https://doi.org/10.1029/2008jd011257, 2009.

Smirnov, A., Holben, B. N., Giles, D. M., Slutsker, I., O'Neill, N. T., Eck, T. F., Macke, A., Croot, P., Courcoux, Y., Sakerin, S. M., Smyth, T. J., Zielinski, T., Zibordi, G., Goes, J. I., Harvey, M. J., Quinn, P. K., Nelson, N. B., Radionov, V. F., Duarte, C. M., Losno, R., Sciare, J., Voss, K. J., Kinne, S., Nalli, N. R., Joseph, E., Moorthy, K. K., Covert, D. S., Gulev, S. K., Milinevsky, G., Larouche, P., Belanger, S., Horne, E., Chin, M., Remer, L. A., Kahn, R. A., Reid, J. S., Schulz, M., Heald, C. L., Zhang, J., Lapina, K., Kleidman, R. G., Griesfeller, J., Gaitley, B. J., Tan, Q., and Diehl, T. L.: Maritime aerosol network as a component of AERONET - first results and comparison with global aerosol models and satellite retrievals, Atmospheric Measurement Techniques, 4, 583-597, https://doi.org/10.5194/amt-4-583-2011, 2011.

Stocker, T.: Climate change 2013: the physical science basis: Working Group I contribution to the Fifth assessment report of the Intergovernmental Panel on Climate Change, Cambridge University Press, 2014.

Tesche, M., Ansmann, A., Muller, D., Althausen, D., Mattis, I., Heese, B., Freudenthaler, V., Wiegner, M., Esselborn, M., Pisani, G., and Knippertz, P.: Vertical profiling of Saharan dust with Raman lidars and airborne HSRL in southern Morocco during SAMUM, Tellus Series B-Chemical and Physical Meteorology, 61, 144-164, https://doi.org/10.1111/j.1600-0889.2008.00390.x, 2009.

Atmos. Meas. Tech. Discuss., https://doi.org/10.5194/amt-2019-132
Manuscript under review for journal Atmos. Meas. Tech.
Discussion started: 4 April 2019

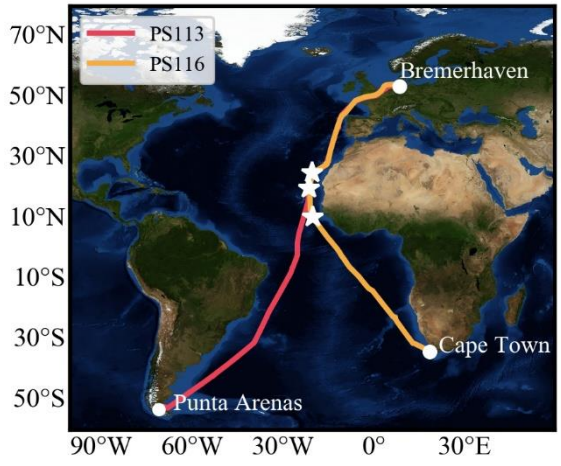

Figure 1. Ship tracks for RV *Polarstern* cruises. PS113 started from Punta Arenas, Chile on 7 May 2018 and arrived at Bremerhaven, Germany on 11 June 2018. PS116 started from Bremerhaven, Germany on 11 December 2018 and arrived at Cape Town, South Africa on 11 December 2018. White stars mark the location of the case studies presented in Sect. 3.

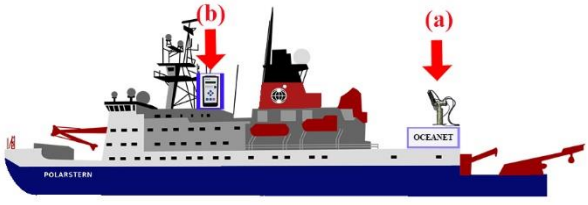

Figure 2 Photometer and lidar observations aboard RV *Polarstern*. MICROTOPS II observations were performed at site (b). Lidar and shipborne CE318-T observations were conducted at site (a).

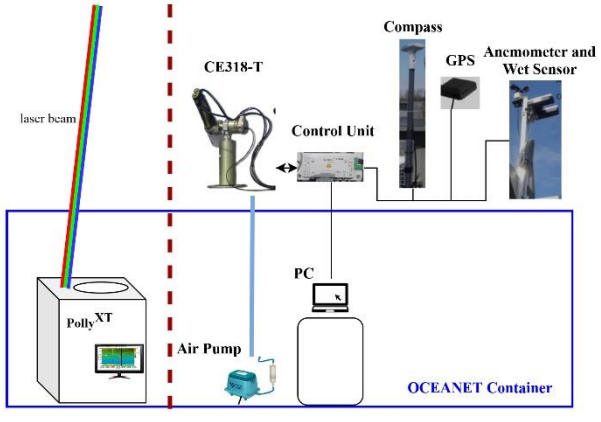

Figure 3. Sketch of the Polly^{XT} lidar (left of the dashed line) and the shipborne CE318-T (right of the dashed line).

Atmos. Meas. Tech. Discuss., https://doi.org/10.5194/amt-2019-132
Manuscript under review for journal Atmos. Meas. Tech.
Discussion started: 4 April 2019

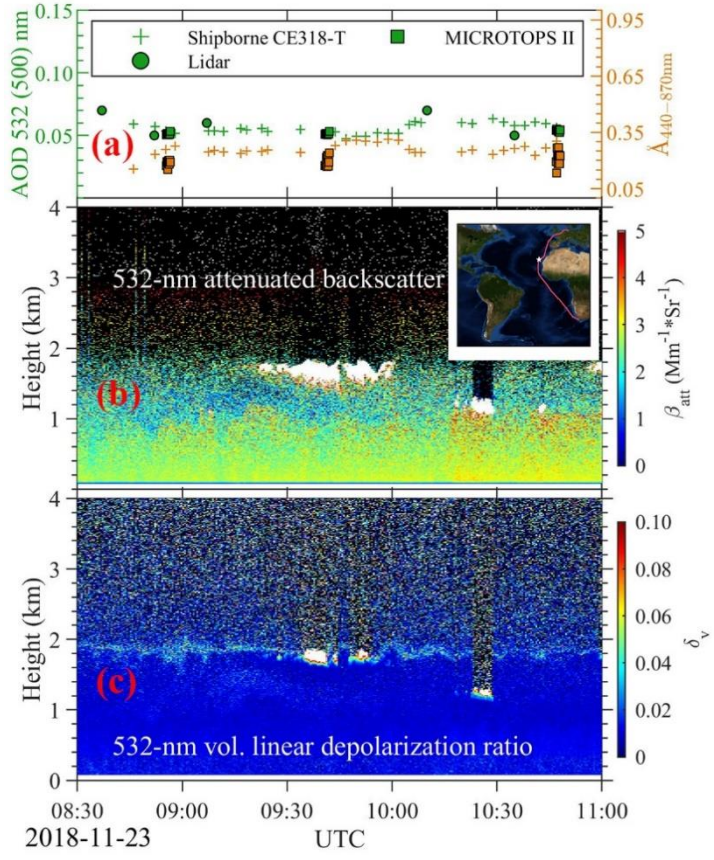

Figure 4. Shipborne aerosol observation with the shipborne CE318-T, MICROTOPS II and Polly^{XT} lidar at pure marine conditions on 23 November 2018. (a) Comparison of 532 nm AOD measured with shipborne CE318-T and Polly^{XT} lidar and 500 nm AOD from MICROTOPS II and Ångström exponent at 440-870 nm from shipborne CE318-T and MICROTOPS II, (b) marine aerosol layer reaching to about 2 km height, partly topped with cumulus clouds (white area), observed with lidar in terms of 532 nm attenuated backscatter, and (c) volume depolarization ratio indicating pure marine condition (very low depolarization ratio caused by the spherical droplets as sea salt particle was deliquescent at RH > 70 %) with dried cubic-like sea salt particles at the top (slightly enhanced depolarization ratio) at RH < 45 %.

Atmos. Meas. Tech. Discuss., https://doi.org/10.5194/amt-2019-132
Manuscript under review for journal Atmos. Meas. Tech.
Discussion started: 4 April 2019

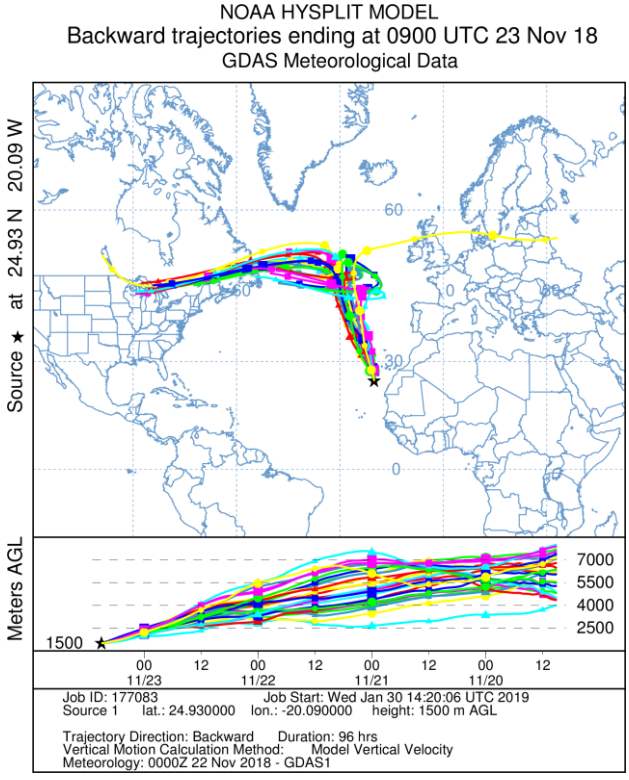

Figure 5. Six-day HYSPLIT backward trajectory ensemble arriving at 1500 m height above RV *Polarstern* (black star, 18.41 °S, 32.93 °W) on 19 May 2018, 22:00 UTC.

Atmos. Meas. Tech. Discuss., https://doi.org/10.5194/amt-2019-132
Manuscript under review for journal Atmos. Meas. Tech.
Discussion started: 4 April 2019

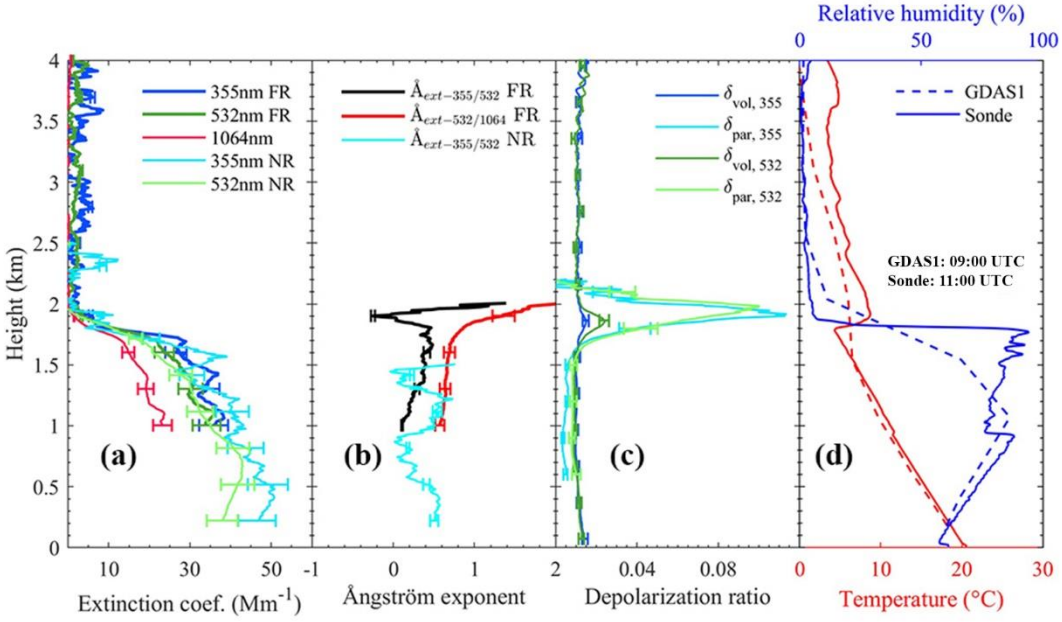

Figure 6 Height profiles of (a) particle extinction coefficient at 355 nm (blue, FR from far-range signal, NR from near-range signal), 532 nm (green), and 1064 nm (red), (b) Ångström exponent computed from different wavelengths pair in (a), (c) volume (δ_{vol}) and particle (δ_{par}) depolarization ratios, and (d) relative humidity (blue) and temperature (red). The lidar observations were taken on 23 November 2018, 08:30 – 09:14 UTC. The radiosonde was launched at 11:00 UTC. GDAS1 data for 09:00 UTC are shown for comparison.

Atmos. Meas. Tech. Discuss., https://doi.org/10.5194/amt-2019-132
Manuscript under review for journal Atmos. Meas. Tech.
Discussion started: 4 April 2019

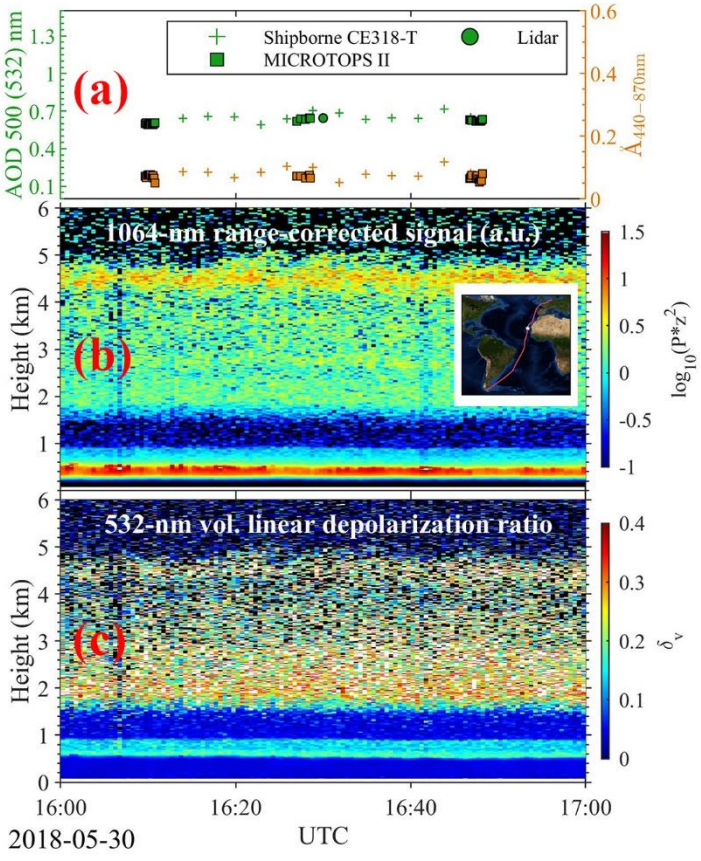

Figure 7. Shipborne aerosol observation with the shipborne CE318-T, MICROTOPS II and Polly^{XT} lidar with strong dust loading on 30 May 2018. (a) Comparison of 500 nm AOD and Ångström exponent at 440-870 nm with shipborne CE318-T and MICROTOPS II, (b) the dust layer extending from 1.5 to 5 km and MBL reaching to 0.6 km, as indicated characterized by the strong range-corrected signal at 1064 nm (red), and (c) volume depolarization ratios indicating the marine layer (low values, blue) and the Saharan dust layer (high values, green and yellow).

Atmos. Meas. Tech. Discuss., https://doi.org/10.5194/amt-2019-132
Manuscript under review for journal Atmos. Meas. Tech.
Discussion started: 4 April 2019

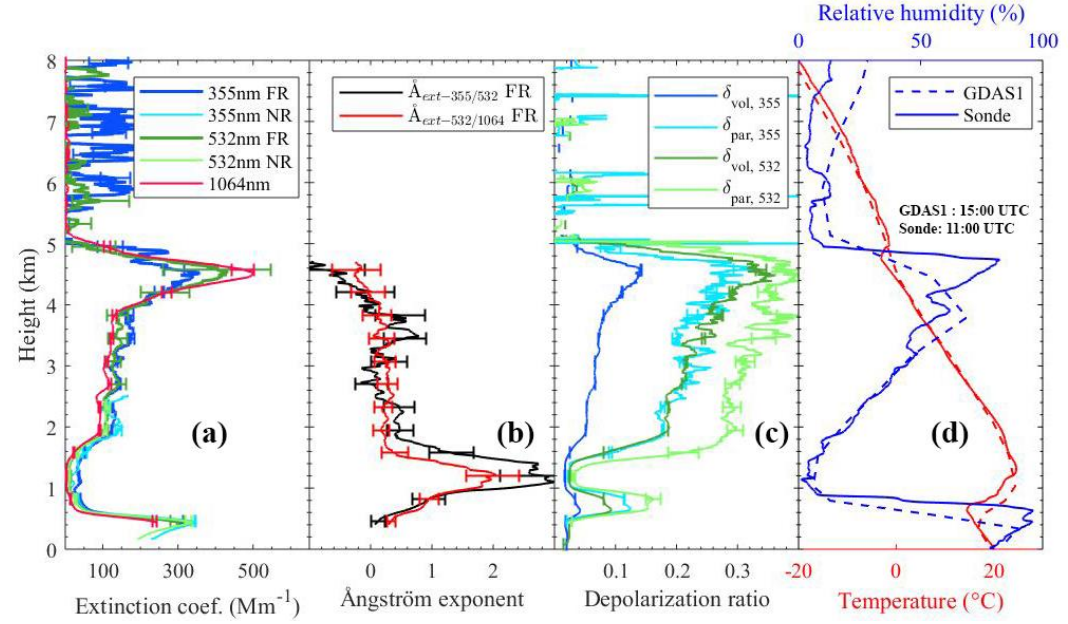

Figure 8. Height profiles of (a) particle extinction coefficient at 355 nm (blue, FR from far-range signal, NR from near-range signal), 532 nm (green), and 1064 nm (red), (b) Ångström exponent computed from different wavelengths pair in (a), (c) volume (δ_{vol}) and particle (δ_{par}) depolarization ratios, and (d) relative humidity (blue) and temperature (red). The lidar observations were taken on 30 May 2018, 16:00 – 16:59 UTC. The radiosonde was launched at 11:00 UTC. GDAS1 data is for 15:00 UTC.

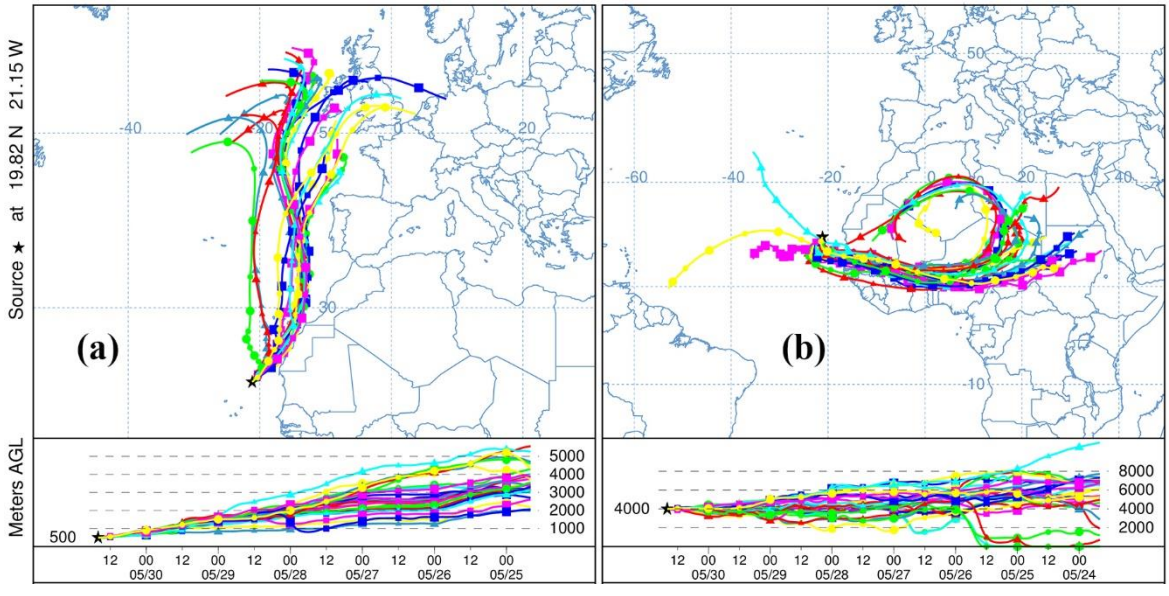

Figure 9. Six-day HYSPLIT backward trajectory ensemble arriving at 500 m (a) and 4,000 m (b) height above RV *Polarstern* (black star) on 30 May 2018, 16:00 UTC.

Atmos. Meas. Tech. Discuss., https://doi.org/10.5194/amt-2019-132
Manuscript under review for journal Atmos. Meas. Tech.
Discussion started: 4 April 2019

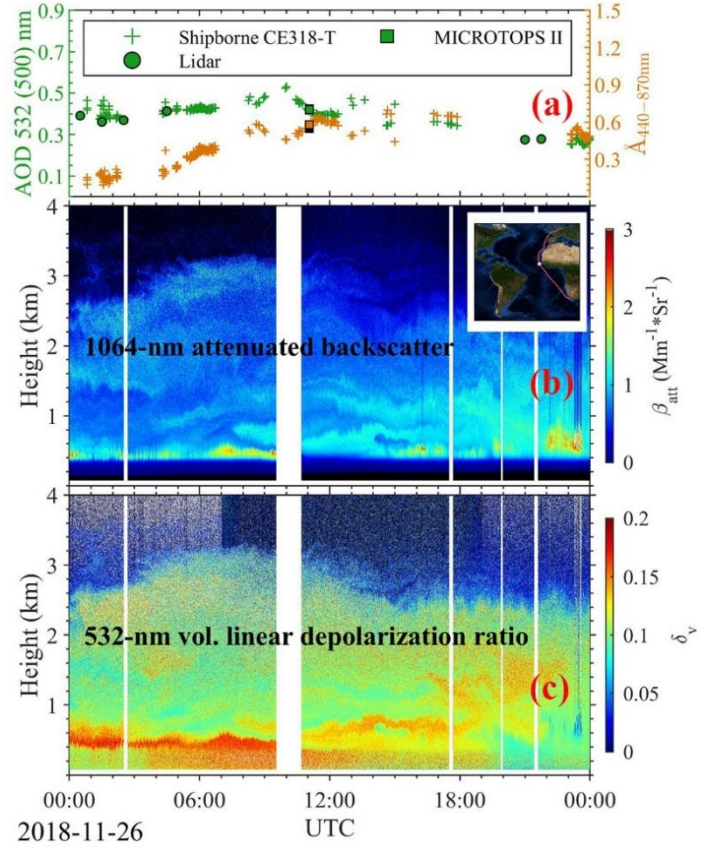

Figure 10. Shipborne aerosol observation with CE318-T, MICROTOPS II and Polly^{XT} lidar at conditions with a mixture of dust and smoke on 26 November 2018. (a) Comparison of 532 nm AOD from shipborne CE318-T and Polly^{XT} lidar observations and 500 nm AOD from MICROTOPS II measurements and Ångström exponent at 440-870 nm obtained from shipborne CE318-T and MICROTOPS II data, (b) mixed layer extended to about 3.5 km height as observed with lidar in terms of 1064 nm attenuated backscatter, and (c) volume depolarization ratio indicating dust-contaminated MBL. The narrow white strips are the lidar depolarization calibration periods and the thick white strip at 10:00 UTC is the routine turn-off time to avoid solar damage at noon.

Atmos. Meas. Tech. Discuss., https://doi.org/10.5194/amt-2019-132
Manuscript under review for journal Atmos. Meas. Tech.
Discussion started: 4 April 2019

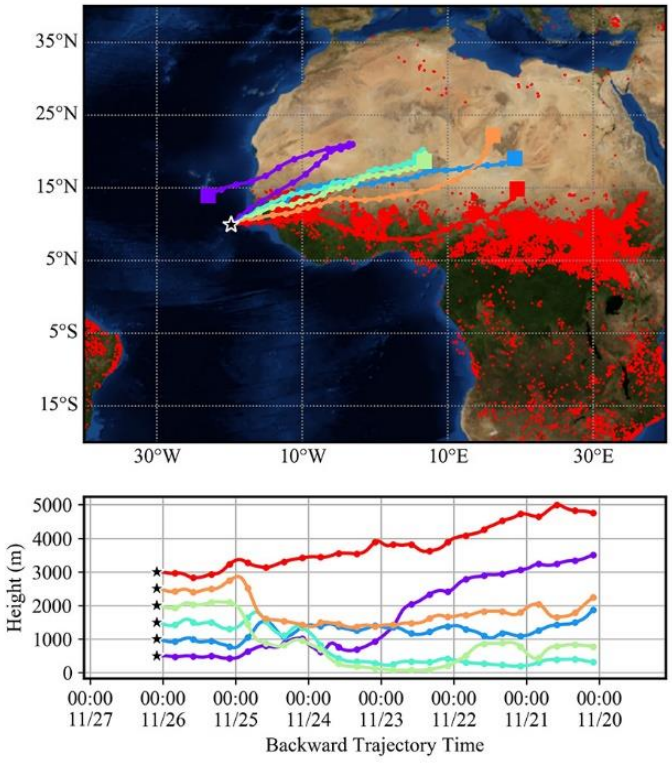

Figure 11. NOAA HYSPLIT backward trajectories arriving at RV *Polarstern* (black star with white border, 10.04 °N, 19.82 °W) on 26 November 2018, 02:00 UTC. Red dots are the fire spots detected by MODIS aboard the Terra and Aqua satellites over the period from 20 November to 26 November 2018 (last access: 4 February 2019).

Atmos. Meas. Tech. Discuss., https://doi.org/10.5194/amt-2019-132
Manuscript under review for journal Atmos. Meas. Tech.
Discussion started: 4 April 2019

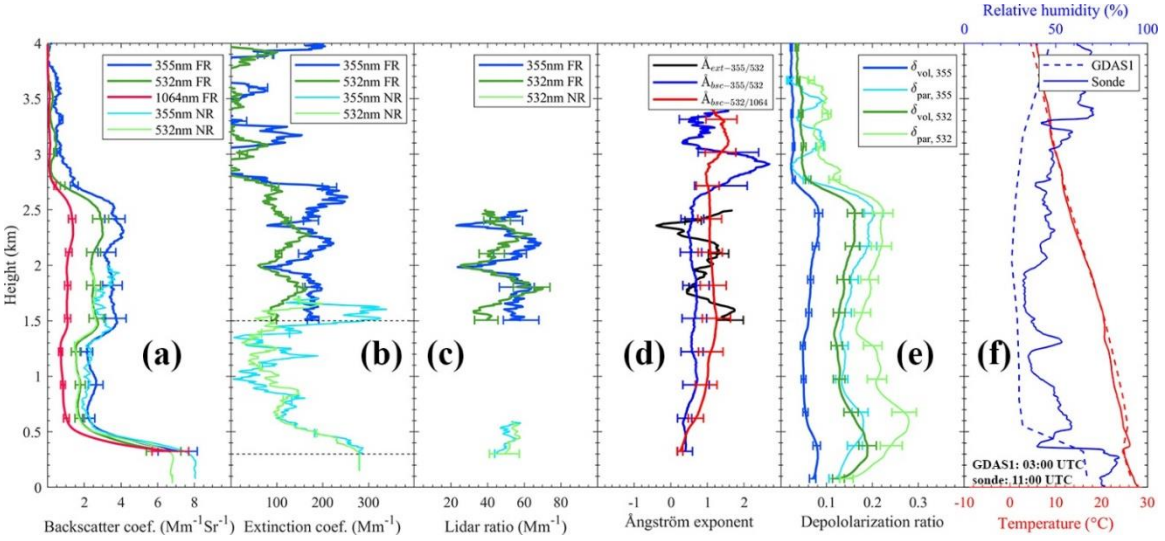

Figure 12. Raman lidar observation on 26 November 2018, 02:00-03:00 UTC. (a) Particle backscatter coefficient, (b) particle extinction coefficient (Raman lidar method), (c) lidar ratio, (d) Ångström exponent computed from different wavelengths pair in (a) and (b), (e) volume (δ_{vol}) and particle (δ_{par}) depolarization ratios, and (f) relative humidity (blue) and temperature (red) from radiosonde observations and GDAS1 dataset.

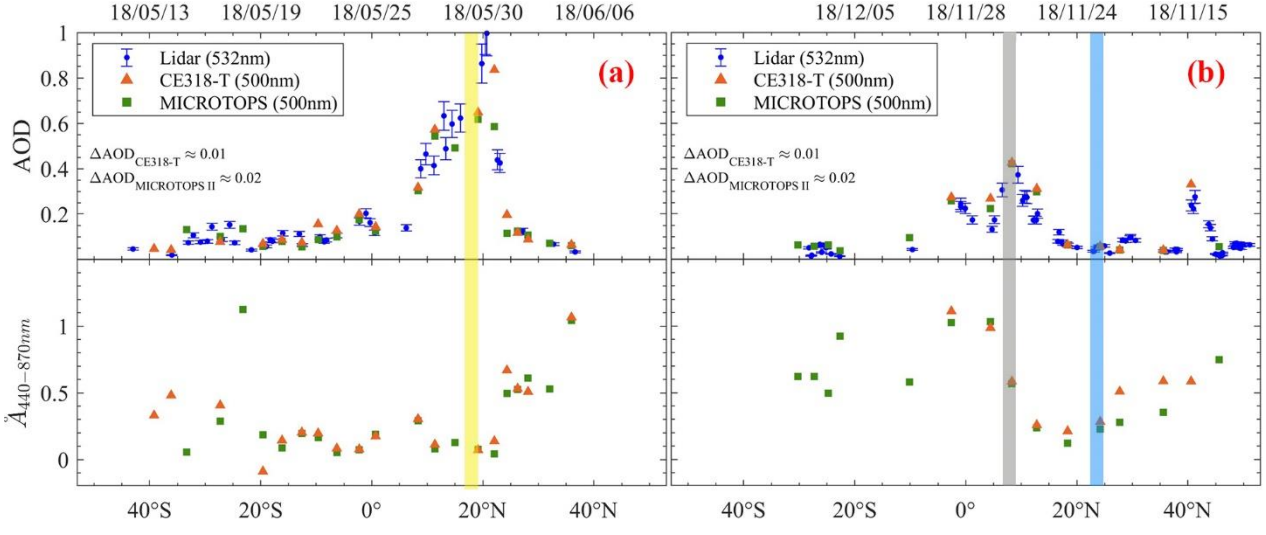

Figure 13. (a) Latitudinal distribution of daily mean AOD measured with Polly^{XT} lidar, MICROTOPS II and shipborne CE318-T. Panel (a) and (b) show the results from PS113 and PS116, respectively. The three colored vertical strips indicate the three cases used in Sect. 3.1 (yellow: Saharan dust in Fig. 7, grey: diurnal measurements in Fig. 10, red: pure marine condition in Fig. 4). Uncertainty in shipborne CE318-T and MICROTOPS II observations are referred to the analysis of Smirnov et al. (2009) and Smirnov et al. (2011).

Atmos. Meas. Tech. Discuss., https://doi.org/10.5194/amt-2019-132
Manuscript under review for journal Atmos. Meas. Tech.
Discussion started: 4 April 2019

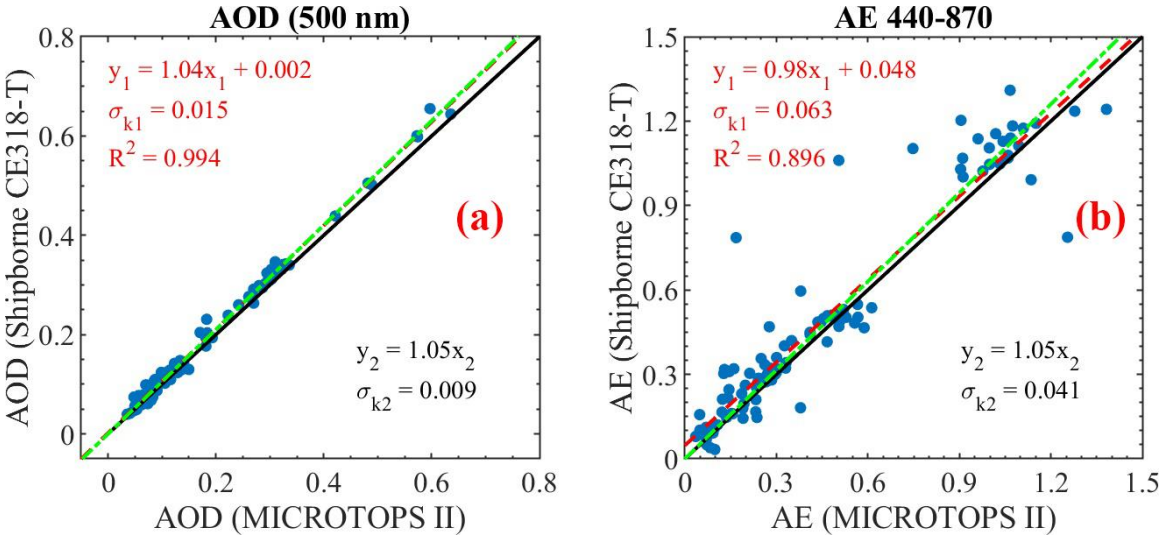

Figure 14. Linear regression of AOD (a) and Ångström exponent (b) from the shipborne CE318-T and MICROTOPS II observations. The data points are the mean values within a sliding window of 20 min. 115 data pairs are used in this regression. The red dashed line is the regression result with free intercept relationship and the green dot-dashed line represents the regression relationship with forced intercept through 0.